JOURNAL OF Materials CHEMISTRY

Pyrrole and polypyrrole-based liquid crystals containing azobenzene mesogenic groups

Yu Chen,[a] William T. A. Harrison,[a] Corrie T. Imrie[a] and Karl S. Ryder*[b]

[a]*Department of Chemistry, University of Aberdeen, Meston Walk, Old Aberdeen, UK AB24 3UE*
[b]*Department of Chemistry, Loughborough University, Loughborough, UK LE11 3TU. E-mail: k.s.ryder@lboro.ac.uk*

Received 5th July 2001, Accepted 3rd November 2001
First published as an Advance Article on the web 30th January 2002

Here we discuss the thermotropic and electrochemical properties and polymerisation of a series of *N*-substituted pyrrole monomers bearing mesogenic 4-substituted azobenzene attached as a pendant group *via* alkyl spacers. We discuss the effect upon these molecular properties of chain length and substitution of the azobenzene moiety with methoxy, cyano and nitro terminal groups. Additionally we present here the first crystal structure determination and analysis of two *N*-alkylpyrroles bearing mesogenic groups.

Introduction

A large proportion of the recent research effort associated with conducting polymers has focussed upon the drive towards crystalline and liquid crystalline materials. This effort is motivated both by an academic interest in the orthogonal conductivity mechanisms of organic conductors, that are convoluted in amorphous systems, and by the potential for technological application in novel device design. New devices and applications are expected to exploit the electronic anisotropy of crystalline and liquid crystalline materials that is a corollary of the structural anisotropy inherent in ordered phases.[1] Such applications will include polymer displays and small scale integrated switching components for information storage in all-polymer memory circuitry. As part of this research effort, and in the continuing search for conducting liquid crystal polymers, much interest has been directed at thiophene and particularly at pyrrole-based systems.[2–13] In our studies focussed on pyrrole systems we have sought to investigate the influence of molecular structure on the thermotropic behaviour of the monomer species and to channel this understanding into the design and fabrication of liquid crystal polymer materials. Our research has centred on the attachment, *via* an alkyl chain, of a mesogenic group to the *N*-site of the pyrrole ring to yield mesogenic monomers and the subsequent polymerisation of these to give side group liquid crystal polymers based on a conducting pyrrole backbone.[12,13] Although the clearing temperatures of *N*-substituted monomers are sometimes lower than those of the analogous 3-substituted materials, presumably implying hydrogen bonding in the latter,[12] there are advantages associated with *N*-substitution. The *N*-substituted pyrroles are symmetrical molecules and hence lead to polymers having regular structures. This is in contrast to the irregular polymeric structures obtained on polymerising 3-substituted pyrrole monomers. Substitution at the *N*-site is also more versatile and the synthetic chemistry is more straightforward.

Despite the growing number of studies on pyrrole-based liquid crystals,[2–13] there is no clear understanding of how molecular structure effects the mesogenic behaviour in this class of materials which are very different in nature to conventional low molar mass liquid crystals. In this respect we have undertaken a systematic study of monomeric molecular species. Here we report the properties of a range of pyrrole-based systems having differing mesogenic groups based on azobenzene. Fig. 1 shows the range of compounds addressed in this study and these are referred to using the acronym *n*-X, where *n* refers to the number of methylene groups in the alkyl spacer chain and x the terminal group on the azobenzene unit. Additionally, we report the preparation and properties of one monomer in which both β-positions carry substituents in order to prevent side-reactions during polymerisation; this is referred to as 3,4-sub-11-OMe (see Fig. 1).

We also describe here, for the first time, the crystal structure determination of two molecular species, 3-CN and 3-NO_2 (see Fig. 1). This represents a significant contribution to the research area, since there are relatively few crystal structure determinations for *N*-alkyl substituted pyrrole species (and fewer still have mesogenic groups), and raises some interesting questions about the nature and mechanism of solid-state polymerisation.

Finally we describe the oxidative polymerisation of these monomers using chemical and electrochemical methods. The polymers are referred to as p(*n*-X).

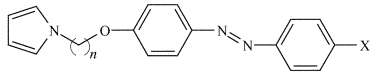

	X	Acronym
$n = 3$	NO_2	**3-NO_2**
$n = 11$	NO_2	**11-NO_2**
$n = 3$	OMe	**3-OMe**
$n = 11$	OMe	**11-OMe**
$n = 3$	CN	**3-CN**
$n = 11$	CN	**11-CN**

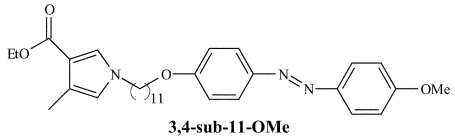

3,4-sub-11-OMe

Fig. 1 The structures of the pyrrole-based monomers and the acronyms used to refer to them.

Experimental

Monomer synthesis

The monomers were prepared using the synthetic route shown in Scheme 1. The syntheses of the α-bromo-ω-[4-(4′-substituted phenylazo)phenyloxy]alkanes have been described in detail elsewhere.[14–16] The *N*-{ω-[4-(4′-substituted phenylazo)phenyloxy]alkyl}pyrroles were prepared using a modification[12] of the procedure reported by Ibison *et al.*[5] Thus only representative characterisation data are provided.

***N*-{3-[4-(4′-Methoxyphenylazo)phenyloxy]propyl}pyrrole, 3-OMe.** Appearance: yellow powder; yield: 44%; melting point: 125 °C.

FT-IR (KBr disk), ν_{max}/cm^{-1}: 3108, 3066 (C–H, Ar); 2944, 2879 (C–H, alkyl); 1601, 1497 (C=C, Ar); 1245, 1150, 1020 (C–O–C, C–O–Ar); 844 (C–H out-of-plane, Ar); 729 (C–H out-of-plane, pyrrole).

^{1}H NMR ($CDCl_3$), δ (ppm): 7.87 (m, 4H, aromatic), 6.99 (m, 4H, aromatic); 6.66 (t, J = 2 Hz, 2H, pyrrole), 6.14 (t, J = 2 Hz, 2H, pyrrole), 4.13 (t, J = 6 Hz, 2H, NCH_2), 3.96 (t, J = 6 Hz, 2H, OCH_2), 3.88 (s, 3H, OCH_3), 2.24 (quintet, J = 6 Hz, 2H, $CH_2CH_2CH_2$).

Elemental analysis: $C_{20}H_{21}N_3O_2$ (336.44). Calcd: C, 71.39; H, 6.30; N, 12.79%. Found: C, 71.56; H, 6.13; N, 12.57%.

Mass spec: m/z 336.2 ($[M + H]^+$), calcd 336.4.

***N*-{11-[4-(4′-Methoxyphenylazo)phenyloxy]undecyl}-3-methylpyrrole-4-carboxylate ethyl ester, 3,4-sub-11-OMe.** 3,4-sub-11-OMe was prepared in an identical manner to that described for the *N*-{ω-[4-(4′-substituted phenylazo)phenyloxy]alkyl}pyrroles but using 3-methylpyrrole-4-carboxylate ethyl ester in place of pyrrole. The synthesis of this molecule has been described elsewhere.[17]

Appearance: yellow powder; yield: 47%; melting point: 88 °C.

FT-IR (KBr disk), ν_{max}/cm^{-1}: 3125, 3068 (C–H, Ar); 2927, 2850 (C–H alkyl); 1686 (C=O); 1600, 1500 (C=C, Ar); 1248, 1146, 1023 (C–O–C, C–O–Ar); 842 (C–H out-of-plane, Ar).

^{1}H NMR ($CDCl_3$), δ (ppm): 7.86 (m, 4H, aromatic), 7.20 (d, J = 2 Hz, 1H, pyrrole), 6.98 (m, 4H, aromatic), 6.35 (q, J = 1 Hz, 1H, pyrrole), 4.25 (q, J = 7 Hz, 2H, CH_2CH_3), 4.02 (t, J = 6 Hz, 2H, NCH_2), 3.88 (s, 3H, OCH_3), 3.76 (t, J = 7 Hz, 2H, OCH_2), 2.24 (d, J = 1 Hz, 3H, C-CH_3), 1.75 (m, 4H, NCH_2CH_2, OCH_2CH_2), 1.55–1.27 (m, 17H, CH_2CH_3), -$(CH_2)_7$-).

Elemental analysis: Calcd: C, 71.86; H, 8.12; N, 8.04%. Found: C, 71.34; H, 8.01; N, 7.74%.

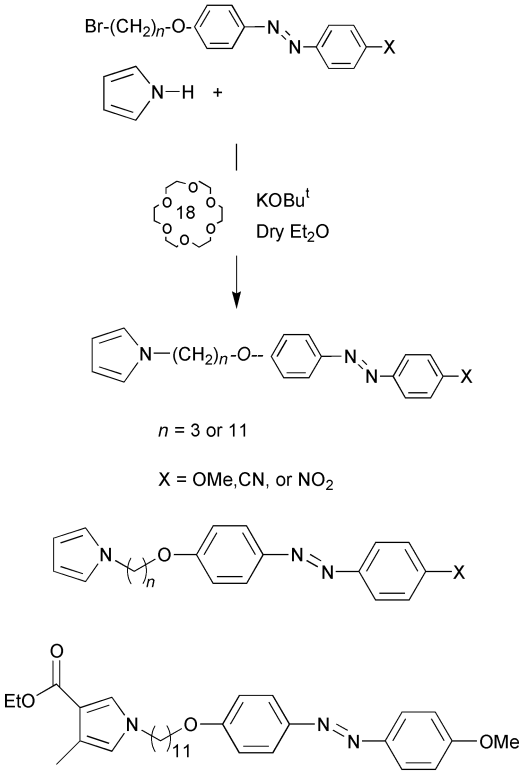

Scheme 1

Polymer synthesis

(a) Chemical polymerisation using iron chloride. The monomer (0.001 mol) in chloroform (5 ml, freshly distilled) was added dropwise to a suspension of anhydrous $FeCl_3$ (0.113 g, 0.7 mol) in chloroform (50 ml, freshly distilled) under nitrogen. The mixture was stirred at room temperature for 24 h. The polymer in solution was then precipitated by addition of excess methanol. The precipitate was extracted using boiling absolute ethanol and the solvent decanted. This procedure was repeated until no unreacted monomer could be detected by thin layer chromatography (TLC) in the filtrate. The precipitate was collected and dried under vacuum. Polymer yields range from 22% (p(3-CN)) to 60% (p(11-NO_2)). The infrared spectra of the polymers were very similar to those of the corresponding monomers except for the absence of the bands at *ca.* 720–740 cm^{-1}. No polymeric material was obtained for the reaction using 3,4-sub-11-OMe.

(b) Chemical polymerisation using iodine. The monomer (0.001 mol) was finely divided and spread over the base of a small beaker and exposed to saturated iodine vapour at room temperature for two days. The excess iodine was removed under vacuum at 60 °C over 2 h. The unreacted monomer was removed using the same method as described in the previous section. The infrared spectra of these polymers were indistinguishable from those obtained using anhydrous iron chloride as the oxidant. Again no polymer was obtained using the monomer 3,4-sub-11-OMe.

(c) Electrochemical polymerisation. Cyclic voltammetry of the *N*-{ω-[4-(4′-substituted phenylazo)phenyloxy]alkyl}pyrroles was performed in acetonitrile solution containing 0.01 M monomer and 0.05 M $[Bu_4N][BF_4]$ with a potential scan rate between 75 and 200 mV s^{-1} on a Au or Pt disc (4 mm diameter). The film electrodes of poly(*N*-substituted pyrrole)s were prepared with 10 cycles of potential scan between −0.4 V and 1.0 V (*versus* ferrocinium/ferrocene as an internal standard), and were rinsed well using acetonitrile then transferred to a monomer free acetonitrile solution for cyclic voltammetric analysis.

The poly(*N*-substituted pyrroles) used for the measurement of reflectance FT-IR spectroscopy, thermogravimetric analysis (TGA), scanning electron microscopy (SEM) and conductivity were prepared on a 3 cm^2 gold foil electrode chronoamperometrically at a static potential of +1.0 V (*versus* ferrocinium/ferrocene as an internal standard) in acetonitrile solution containing 0.01 M monomer and 0.05 M $[Bu_4N][BF_4]$. The films on the gold foil were washed with industrial methylated spirit (IMS) and acetone and then dried in air.

The polymer film thicknesses for FT-IR spectral analysis and surface conductivity measurements were controlled by chronocoulometric growth. Typical film thicknesses of 4–5 μm were achieved by passing 1.1 C cm^{-2} charge during the polymerisation.

The poly(*N*-substituted pyrrole)s for UV-visible spectroscopy were prepared on a 2 × 1 cm ITO glass electrode with 20 potential cycles between −0.4 and +1.0 V (*versus* ferrocinium/ferrocene as an internal standard) in acetonitrile solution containing 0.01 M monomer and 0.05 M $[Bu_4N][BF_4]$. After 20 cycles a polymeric film had been deposited on the ITO

electrode, which was washed with IMS and acetone and then dried in air.

Characterisation

^{1}H and ^{13}C NMR data were obtained on Varian *Unity Inova* 400 MHz and Bruker AC-F 250 MHz spectrometers. FT-IR spectra were recorded using a Nicolet 205 FT-IR spectrometer; polymer film spectra were recorded *ex situ* using a specular reflectance accessory at an incident angle of 45°, or samples were prepared as KBr pressed films. In order to prevent spectral baseline distortion caused by conduction band effects the polymer samples were prepared in their fully reduced form. Mass spectra were recorded on a Finnigan MassLab Navigator. The thermal properties of the materials were determined by differential scanning calorimetry (DSC) using a Mettler Toledo 821 Differential Scanning Calorimeter at a heating/cooling rate of 10 °C min^{-1} under a constant flow of nitrogen and calibrated using indium. Phase identification was performed by polarised light microscopy using an Olympus BH-2 optical microscope equipped with a Linkam THMS 600 heating stage and TMS91 control unit.

All electrochemical procedures were carried out using an EG & G Princeton Applied Research potentiostat/Galvanostat Model 263A driven by the M270 software package. A conventional three-electrode system was used in a single compartment cell. A 0.05 M solution of $[NBu_4][BF_4]$ (recrystallised from diethyl ether) in dry acetonitrile (distilled over CaH_2) was used as a supporting electrolyte. The solutions were deoxygenated by bubbling dry argon for 5 minutes before each measurement and all experiments were carried out under an argon atmosphere. An AgCl/Ag wire electrode was used as a reference in each experiment and this was calibrated at the end of the experiment by addition of ferrocene as an internal standard. A large platinum flag was used as a counter electrode. A gold foil (3.0 cm^2) was used as a working electrode for electropolymerisation of films for FT-IR spectroscopy or conductivity measurements. A Pt, or Au disc (4 mm dia.) was used as a working electrode for cyclic voltammetry experiments. All electrodes were cleaned by polishing with an aqueous slurry of 10 μm and 3 μm alumina before use.

The surface conductivities of electrochemically grown films were measured using a custom built dc linear four point probe apparatus with a Keithley Instruments high impedance electrometer as described in detail elsewhere.[12,18] For the conductivity measurements, pellets (1 cm diameter) were prepared of the polymers by pressing the sample (*ca.* 50 mg) under 5 ton for 30 min.

Results and discussion

Thermal behaviour of monomers

The transitional properties of the *N*-{ω-[4-(4′-substituted phenylazo)phenyloxy]alkyl}pyrroles are listed in Table 1. All

Table 1 Transitional behaviour of the *N*-{ω-[4-(4′-substituted phenylazo)phenyloxy]alkyl}pyrroles, (*n*-X). Brackets denote monotropic transitions

Sample	T_{CrI}/ °C[a]	ΔH_{CrI}/ kJ mol^{-1}	T_{NI}/ °C[b]	ΔH_{NI}/ kJ mol^{-1}	$\Delta S_{NI}/R$
3-OMe	125	44.8	(83)	0.99	0.34
11-OMe	105	65.3	(77)	1.79	0.62
3,4-sub-11-OMe	88	57.7	(53)		
3-NO_2	143	33.4	<50		
11-NO_2	79	37.7	(68)	0.52	0.18
3-CN	147	36.7	(75)		
11-CN	102	59.6	(76)		

[a]Extracted from the DSC reheat trace. [b]Measured using the polarised light microscope.

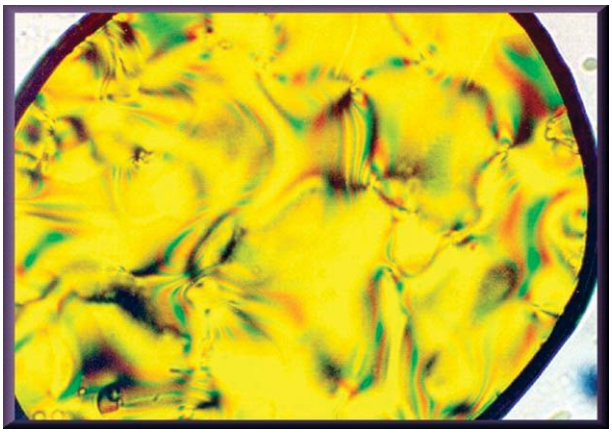

Fig. 2 Nematic Schlieren texture exhibited by 11-OMe at 60 °C.

the compounds with the exception of 3-NO_2 exhibited a monotropic nematic phase identified on the basis of the characteristic Schlieren texture when viewed through the polarised light microscope (see Fig. 2). The entropy changes associated with the clearing transition, expressed as the dimensionless quantity $\Delta S_{NI}/R$, are consistent with this assignment. The clearing temperatures were difficult to measure accurately, not only as a result of the strongly monotropic behaviour, but also because these materials exhibit clearing behaviour at temperatures *below* the nematic-isotropic transition temperature, T_{NI}. This transition is driven by the *trans–cis* photoisomerisation of the azobenzene unit. Thus, in the bent *cis* form T_{NI} is considerably reduced compared with the T_{NI} of the rod-like *trans* form. This is a reversible process and turning off the microscope light resulted in the reappearance of the nematic phase. Similar behaviour has been observed for a range of azobenzene-containing systems, including thiophene-derivatives.[19]

For each pair of homologues the melting point of the undecyl homologue is considerably lower than that of the propyl homologue. This presumably reflects the increase in the conformational component of the melting entropy on increasing the alkyl chain length. By contrast the nematic-isotropic transition temperatures of 3-OMe and 11-OMe and 3-CN and 11-CN are very similar. This is conventional behaviour for liquid crystal series having clearing temperatures of *ca.* 100 °C. To understand this behaviour we must consider the effects of increasing the length of the alkyl chain.[20] On one hand, the anisotropic properties of the molecule are increased resulting in an increased T_{NI} while on the other, the interactions between the mesogenic units are diluted resulting in a decreased T_{NI}. Thus the overall effect of increasing the chain length will depend on the interaction strength parameter of the mesogenic groups. For strongly interacting units the dilution effect dominates and the clearing temperatures fall whereas for more weakly interacting units the increase in molecular anisotropy dominates and the clearing temperatures rise. It is found experimentally that these two effects are essentially balanced for series with clearing temperatures of *ca.* 100 °C and thus increasing chain length has little effect. We note that this explanation has not included a discussion of the odd–even effect but this is not relevant here as the 3-X and 11-X homologues have similar shapes.[12] The clearing temperature of 11-NO_2 is somewhat lower than those of 11-OMe and 11-CN implying a lower interaction strength parameter between the mesogenic units. Thus, increasing the chain length in the *n*-NO_2 series should have a more pronounced effect on the clearing temperature and this is indeed observed. Specifically, the T_{NI} of 3-NO_2 is considerably lower than that of either 3-OMe or 3-CN.

Table 1 also lists the transitional properties of 3,4-sub-11-OMe

which exhibits a monotropic nematic phase. Both the melting and clearing temperatures of 3,4-sub-11-OMe are considerably lower than those of 11-OMe reflecting the decrease in molecular anisotropy.

It is interesting to note that the T_{NI} of a 3-substituted pyrrole-based monomer containing a hexyl alkyl spacer and the methoxyazobenzene unit is 77 °C,[7] and is similar, therefore, to the T_{NI}s of 3-OMe and 11-OMe. By contrast with materials containing cyanobiphenyl as the mesogenic unit, the T_{NI} of the 3-substituted pyrrole is considerably higher.[12] As we have already noted, this was attributed to the formation of supramolecular hydrogen bonded extended chains[21] in which the nitrile group acted as the hydrogen bond acceptor and the pyrrole unit the hydrogen bond donor.[12] This view is supported by the behaviour of the methoxyazobenzene containing monomers for which no hydrogen bond acceptor is present. Thus we would expect the clearing temperatures of the 3- and *N*-substituted homologues, which are essentially identical in shape,[12] to be similar as indeed they are.

Chemical polymerisation

The monomers were polymerised using either iron(III) chloride in homogeneous solution, or iodine vapour in contact with the monomer in the solid phase, as oxidant. A low mole ratio of iron chloride : monomer (0.7 : 1) was used because it has been reported that for higher mole ratios (2.3 : 1) infusible, high molecular weight and high polydispersity materials were obtained.[4] Polymers were obtained from all the monomers except 3,4-sub-11-OMe. Despite this, we have been able to produce copolymers of 3,4-sub-11-OMe with unsubstituted pyrrole using similar techniques from a solution containing a binary mixture of monomers. These results suggest that the growth of homopolymers of 3,4-sub-11-OMe is inhibited by steric interactions involving the substituents on the β-sites. Such interactions would act to stabilise the dimeric or oligomeric radical cations preventing the formation of polymeric materials. All other polymers obtained were insoluble in common organic solvents strongly suggesting either very high molecular weight material or the existence of crosslinking through the β-positions of the pyrrole units.

All the polymers prepared either by chemical or electrochemical means exhibited relatively low electronic conductivity ($\sigma < 10^{-4}$ S cm^{-1}) and decomposed prior to melting. Thus no liquid crystalline behaviour was observed.

Electrochemical behaviour of monomers

The redox behaviour of the monomers in this series was characterised using cyclic voltammetry at a conventional (mm scale) solid electrode interface in common organic solvents *e.g.* acetonitrile or CH_2Cl_2. The cyclic voltammetry data for 11-NO_2 in acetonitrile at a Pt disk electrode are summarised graphically in Fig. 3. These data show four discrete redox processes, two oxidations and two reductions. In the anodic scan, Fig. 3a, two irreversible multi-electron processes are visible at $E = +550$ mV and $E = +1000$ mV *versus* ferrocinium/ferrocene as an internal standard. The first of these processes is associated with the irreversible oxidation of the pyrrole moiety and successive repetitive scans between -840 mV and +660 mV results in the emergence of a new quasi-reversible couple at $E = -40$ mV, Fig. 3b, that is attributed to the growth and redox behaviour of the polymer on the electrode surface. Often the voltammetric peak for oxidation of substituted pyrroles is not observed at moderate potential scan rates because of the very rapid following chemistry associated with polymerisation. In this case the manifestation of the voltammetric peak at relatively slow scan rates suggests that the rate of polymerisation is sluggish compared, for example, with *N*-methylpyrrole, or unsubstituted pyrrole. This is likely

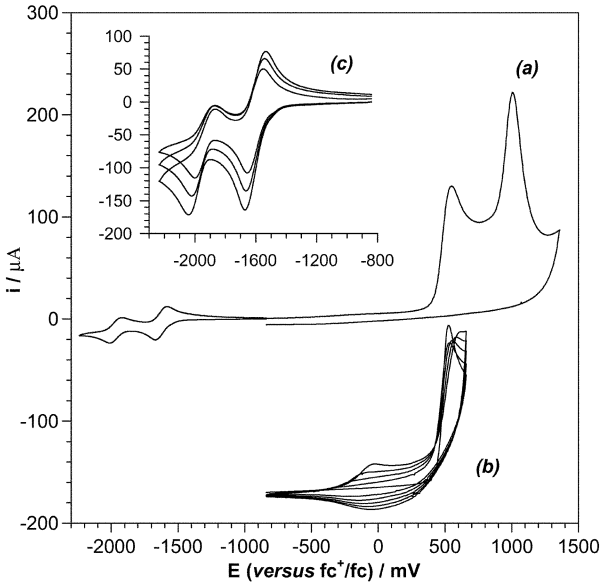

Fig. 3 Cyclic voltammetry of 11-NO_2 at a Pt disk electrode in MeCN using a potential scan rate $v = 75$ mV s^{-1}; (*a*) anodic scan between −840 mV and +1360 mV, (*b*) 5 repetitive anodic scans between −840 mV and +650 mV, (*c*) cathodic scan between −840 mV and −2240 mV, varying scan rate 100 mV s^{-1} $< v >$ 200 mV s^{-1}. The potential is measured with respect to ferrocinium/ferrocene as an internal standard.

to be the result of the steric constraints inflicted upon the pyrrole moiety by the large mesogenic substituent and is consistent with our previous observations.[12] The second anodic feature is much narrower than the first and more symmetrical in shape. The resultant linear plot of anodic peak height *versus* scan rate confirmed that this process is dominated by surface adsorption rather than diffusion. This feature is assigned to the irreversible oxidation of the azobenzene moiety of the mesogenic group. Subsequent addition of small amounts of 1-bromo-11-[4-(4′-nitrophenylazo)phenyloxy]undecane to the cell solution caused a concomitant increase in the feature at $E = +1000$ mV but the peak at $E = +550$ mV remained unaffected. This observation is consistent with our assignment and also suggests that the process does not occur within the newly formed polymer deposited on the electrode surface.

These two features observed in the anodic regime for 11-NO_2 were common to all the species studied here. Variations in peak potential for oxidation of the pyrrole moiety, in particular, were minor, however, and reflect the magnitude of the electronic influence exerted upon the pyrrole ring system by the terminal substituent of the mesogenic group.

The cathodic regime in the voltammetry of 11-NO_2 revealed two reversible couples at $E = -1630$ mV and $E = -1960$ mV, Fig. 3c. These correspond to the one electron reductions of the nitro and azobenzene moieties, respectively, of the mesogenic group. Separate additions of small quantities of *p*-nitrotoluene and 1-bromo-11-[4-(4′-cyanophenylazo)phenyloxy]undecane to the cell solution were made to confirm these assignments. Addition of *p*-nitrotoluene caused an increase only in the relative peak height of the couple at $E = -1630$ mV (and also slight broadening because the redox potentials of the nitro moiety in each species are not exactly coincident) whilst addition of 1-bromo-11-[4-(4′-cyanophenylazo)phenyloxy]undecane caused a concomitant increase only in the redox couple at $E = -1960$ mV.

Both cathodic redox couples show reversible behaviour at slow scan rates ($v < 75$ mV s^{-1}), however, on increasing the potential scan rate both couples exhibit peak broadening and a concomitant increase in peak separation that together define pseudo-reversible behaviour. This is probably caused by slow heterogeneous electron transfer kinetics at the Pt electrode but we have made no attempt to determine the rate constants here.

Table 2 Crystallographic parameters

	3-CN	3-NO_2
Empirical formula	$C_{20}H_{18}N_4O$	$C_{19}H_{18}N_4O_3$
Formula weight	330.38	350.37
Crystal system	Triclinic	Monoclinic
a/Å	9.5009 (6)	11.8709 (18)
b/Å	13.9016 (9)	7.6449 (12)
c/Å	14.6728 (10)	20.891 (4)
α/°	66.442 (2)	90
β/°	81.618 (2)	111.696 (3)
γ/°	81.938 (2)	90
V/Å^3	1750.3 (2)	1761.6 (5)
Z	4	4
Space group	$P\bar{1}$ (No. 2)	$P2_1/c$ (No. 14)
T/°C	20 ± 2	20 ± 2
λ/Å	0.6923	0.6923
ρ_{calc}/g cm^{-3}	1.25	1.32
μ/mm^{-1}	0.080	0.092
Reflections measured	12705	16650
R_{int}	0.019	0.053
Merged, observed[a] reflections	5899, 4086	4764, 2416
Parameters	449	356
$R(F)^b$	0.079	0.068
$wR(F^2)^c$	0.258	0.198

[a] $I > 2\sigma(I)$ after the merging of systematically equivalent and multiply-measured reflections. [b] $R = \Sigma||F_o| - |F_c||/\Sigma|F_o|$ for observed reflections. [c] $R_w = [\Sigma w(|F_o^2| - |F_c^2|)^2/\Sigma w|F_o^2|^2]$ for all merged reflections.

Interestingly neither cathodic redox couple is observed in the voltammetry of an electrode coated with p(11-NO_2) recorded in a separate solution containing no monomer. This is consistent with our observations on other nitro substituted polypyrroles and other modified electrode systems. The absence of the voltammetric peaks in the voltammetric scans is indicative of very slow charge propagation though the polymer film resulting from slow electron self-exchange between, and restricted diffusion of, electroactive sites within the polymer phase.[22] Consequently the appearance of the voltammogram is dominated by the relationship between the charge propagation kinetics of the film and the time scale of the voltammetric seep. Hence, absence of the cathodic peaks from the cyclic voltammogram of the p(11-NO_2) modified electrode does not necessarily imply absence of the mesogenic group from the polymer material.

Crystal structures of the *N*-substituted pyrroles

Crystal structure data for pyrrole and substituted pyrrole species are relatively scarce and make up only a small proportion of the most recent version of the Cambridge Structural Database.[23] For example, a search through the database for the pyrrole moiety in which both α-positions are unsubstituted, but upon which no other constraints are imposed, reveals only 133 hits from a database containing more than 233000 organic and organometallic structures. Within this subset of crystal structure data there are examples of structures in which pyrrole acts as, or as part of a ligand to metallic systems (in various bonding modes including η-5),[24–26] as a solvent of crystallisation[27] and of novel structures and geometries in which pyrrole moieties play a key role,[28] however, there are very few examples of *N*-alkylpyrrole moieties and none that contain azobenzene mesogenic groups.

Crystals of two of the monomers, 3-CN and 3-NO_2, were of sufficiently good quality to allow for structure determination by single crystal diffraction methods using the synchrotron X-ray diffraction facility [λ = 0.69230 Å as selected by a Si(111) monochromator, T = 293 (2) K, Bruker SMART CCD area detector diffractometer] at SRS beam-line station 9.8 at Daresbury Laboratory, UK.[29] Both structures are in agreement with our formulations (Fig. 1) and with all other spectroscopic data.

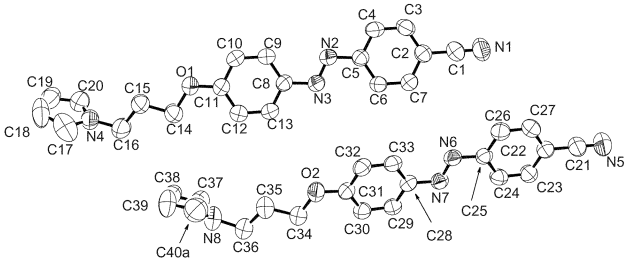

Fig. 4 Asymmetric unit of 3-CN (50% thermal ellipsoids, H atoms omitted for clarity). Only one of the two orientations of the disordered C40 species is shown.

Preliminary scans indicated a triclinic cell for 3-CN and a monoclinic cell for 3-NO_2. Intensity data were collected in narrow-slice ω-scan mode with the aid of the programs SMART and SAINT.[30] Absorption and incident beam decay corrections were applied on the basis of multiple and symmetry-equivalent reflections with the program SADABS.[31] X-Ray scattering factors appropriate to the incident wavelength used were taken.[32] For 3-NO_2 the systematic absences were consistent with space group $P2_1/c$ which was assumed for the remainder of the crystal structure analysis. The initial atomic parameters were derived by direct methods[33] and the remaining non-hydrogen atoms were located from difference maps as the refinements progressed. For 3-CN, one of the pyrrole ring carbon atoms showed excessive thermal motion normal to the plane of the ring and was modelled as being disordered over two sites of equal occupancy. For 3-NO_2, a disorder model was developed to account for two overlapping orientations of the phenyl–azo–phenyl grouping. A similar disordering effect involving a pair of phenyl groups linked through a rigid intermediate unit has been seen elsewhere.[34] Constrained refinement of occupation factors indicated a 0.68(1) : 0.32(1) ratio for the major : minor components in 3-NO_2. All the H atoms were located geometrically and refined[35] by riding on their appropriate N or C atoms. Selected crystallographic data for 3-CN and 3-NO_2 are listed in Table 2.†

Crystal structure of 3-CN

The asymmetric unit contains 2 molecules (molecule **A** including atom N1 and molecule **B** including atom N5) as shown in Fig. 4. The molecules are aligned with the long axis of the unit cell and are oriented essentially parallel to each other. The conformation of the molecules within each asymmetric unit are similar such that the alkyl chain exhibits an all-*trans* linkage pattern. The phenyl rings of the mesogenic units are planar (maximum deviation from best least squares plane $<$0.025 Å) but these planes are rotated with respect to each other by 6.9(2)° and 3.8(2)° for **A** and **B**, respectively. Similarly, the planes containing the pyrrole moieties are rotated from the reference planes containing the cyanophenyl units by 54.2(2)° and 79.4(2)° for **A** and **B**, respectively. The two asymmetric molecules pack in the unit cell in an alternating fashion such that the gap between the pyrrole moieties of one asymmetric grouping is partially occupied by the nitrile head group of a molecule from an adjacent symmetry generated unit. This packing arrangement is shown in Fig. 5. The nearest-neighbour α-pyrrole carbon atom distance is 6.9 Å.

Crystal structure of 3-NO_2

The asymmetric unit for structure 3-NO_2 consists of a single molecule as shown in Fig. 6. The two phenyl rings of the

†CCDC reference numbers 169300 and 169301. See http://www.rsc.org/suppdata/jm/b1/b105976a/ for crystallographic files in .cif or other electronic format.

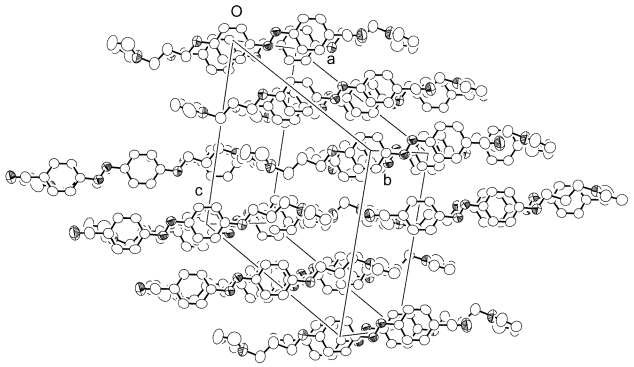

Fig. 5 Packing diagram for 3-CN (50% thermal ellipsoids).

molecule are essentially planar (maximum deviation from best least-squares plane <0.025 Å). The azobenzene moiety is slightly twisted such that although the $O_2N–C_6H_5–N=N–$ structural unit is essentially planar, the plane of the phenyl ring attached to that unit is rotated by 6.0(7)°. The plane of the pyrrole unit is rotated by 64.4(1)° relative to the plane defined by the $O_2N–C_6H_5–N=N–$ grouping. The molecules are stacked within the unit cell in two distinct layers separated by a distance of 7.645 Å, Fig. 7. The layers are distinguished from one another by the orientation of the long axis of the molecule (*i.e.* the line connecting the pyrrole and azobenzene moieties). This axis is rotated by 180° in each successive layer such that a view of the unit cell normal to (100) reveals a lamellar structure with alternate nitro and pyrrole moieties pointing outwards. Within each layer the molecules are arranged in a head to tail fashion so the overall packing describes a three dimensional alternating herringbone type structure. In fact, this molecular packing closely resembles the low-temperature packing of unsubstituted pyrrole,[36] but is quite different to that of *N*-(*p*-nitrophenyl)-pyrrole[37] in which the molecules are all aligned in the same direction. The structure of 3-NO_2 results in nearest-neighbour pyrrole α-carbon atom separations of 3.97 Å between molecules of adjacent layers having opposite orientations. In contrast to the structure of 3-CN the alkyl linkage shows a *gauche* conformation.

In both these structures the separation between neighbouring pyrrole moieties seems to be too large to facilitate solid state polymerisation. However, the nearest neighbour α-pyrrole

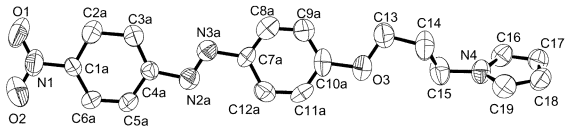

Fig. 6 Asymmetric unit of 3-NO_2 (50% thermal ellipsoids, H atoms omitted for clarity) showing the major orientation of the disordered $–C_6H_4–N=N–C_6H_4–$ entity only (see text).

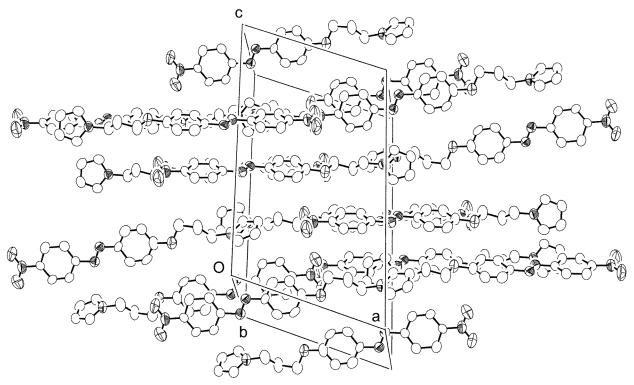

Fig. 7 Packing diagram for 3-NO_2 (50% thermal ellipsoids).

carbon atom distance for 3-NO_2, in particular, is relatively small compared to *N*-(*p*-nitrophenyl)pyrrole,[37] or *N*-phenylsulfonylpyrrole,[38] whose corresponding nearest neighbour distances are 4.56 Å and 4.33 Å respectively. Also, the nearest neighbour α-pyrrole carbon atom distance for 3-NO_2, is, surprisingly, slightly smaller than the equivalent nearest neighbour distance of 4.04 Å in the structure of unsubstituted pyrrole.[36] Consequently it seems likely that the formation of polymeric material following exposure of finely divided powder samples to iodine vapour must involve an interfacial rearrangement of the molecules at the surface of the solid. It is clear that the molecular packing in both structures is determined largely by the mesogenic group. Comparison of the 3-CN and 3-NO_2 crystal structures with analogous non-pyrrole containing azobenzene moieties[39] reveals very similar packing geometries in both cases.

Both structures described here exhibit slight buckling of the pyrrole moiety; whilst these deviations are relatively small, smaller deviations in pseudo planar aromatic structures have been recently reported as resulting from intramolecular crowding.[40,41] This is clearly not the case here so that the observed deviations are probably caused by packing forces within the crystal lattice.

Conclusion

This study has revealed a number of novel and interesting properties of *N*-substituted mesogenic pyrroles although it is clear that these species are unlikely to lead to homopolymers with similar liquid crystal behaviour. All the monomer species studied except 3-NO_2 showed liquid crystal behaviour exhibiting monotropic nematic phases. These nematic phases were light sensitive because of the *cis–trans* isomerisation of the azobenzene moiety. Whilst on the one hand this makes accurate determination of clearing temperatures difficult, on the other hand it presents an opportunity for switching and controlling the anisotropic properties of the ordered phase. It is evident in this study that, from the dependence of clearing temperature on chain length, the interaction strength parameter for the nitroazobenzene moiety is weaker than that for the cyano or methoxy derivatives, and that introduction of additional β-substituents onto the pyrrole ring disrupts the shape anisotropy of the molecule and destabilises the nematic phase. This latter observation is disappointing since these substituents were intended to enhance the stability of the liquid crystal phase in subsequent polymer materials by preventing crosslinking . However, we have also observed here that these same substituents prevent the formation and growth of homopolymer.

The voltammetry of this series of monomers shows several interesting features and all the species with the exception of 11-3-sub-OMe underwent electrochemical oxidation of the pyrrole moiety resulting in polymer film formation.

Our crystal structure data for 3-NO_2 and 3-CN show a number of features that provide insight into the structure of ordered phases containing pyrrole. In particular it is clear that the intermolecular distances in these solid phases are apparently too great to facilitate solid state polymerisation such that some surface rearrangement must be invoked for these polymer materials to form. Furthermore it is interesting, although inconclusive, to note that the *gauche* linkage of the alkyl chain, which leads to a molecular shape with less structural anisotropy than the all-*trans* links, is present only in the species that exhibits no nematic phase, 3-NO_2.

Acknowledgement

The authors gratefully acknowledge the EPSRC (GR/Ll01085) for funding this work. We are also gratefully indebted to Simon

Teat and Elizabeth MacLean (Daresbury Laboratory) for experimental assistance and we acknowledge the provision of time on DARTS, the UK national synchrotron radiation service at the CLRC Daresbury Laboratory, through funding by the EPSRC. We also thank Alan Howie (University of Aberdeen) for his invaluable advice on the crystal structure refinements.

References

1 M. J. Winokur, in *Handbook of Conducting Polymers* 2nd edn., ed. T. A.Skotheim, R. L. Elsenbaumer and J. R. Reynolds, Marcel Dekker, New York, 1998.
2 P. J. Langley, F. J. Davis and G. R. Mitchell, *Mol. Cryst. Liq. Cryst.*, 1993, **234**, 765.
3 D. Melamed, C. Nuckols and M. A. Fox, *Tetrahedron Lett.*, 1994, **35**, 8329.
4 F. Vicentini, J. Barrouillet, R. Laversanne, M. Mauzac, F. Bibonne and J. P. Parneix, *Liq. Cryst.*, 1995, **19**, 235.
5 P. Ibison, P. J. S. Foot and J. W. Brown, *Synth. Met.*, 1996, **76**, 297.
6 H. Hasegawa, M. Kijima and H. Shirakawa, *Synth. Met.*, 1997, **84**, 177.
7 P. J. Langley, F. J. Davis and G. R. Mitchell, *J. Chem. Soc., Perkin Trans.*, 1997, **2**, 2229.
8 M. Kijima, H. Hasegawa and H. Shirakawa, *J. Polym. Sci., Part A:Polym. Chem.*, 1998, **36**, 2691.
9 C. Jego, E. Dupart, P. A. Albauy and C. Mingotaud, *Thin Solid Films*, 1998, **329**, 1.
10 B. Faye, M. Mauzac and J. P. Parneix, *Synth. Met.*, 1999, **99**, 115.
11 M. Kijima, S. Abe and H. Shirakawa, *Synth. Met.*, 1999, **101**, 61.
12 Y. Chen, C. T. Imrie and K. S. Ryder, *J. Mater. Chem.*, 2001, 990.
13 Y. Chen, C. T. Imrie and K. S. Ryder, *J. Mater. Sci. Lett.*, in the press.
14 C. T. Imrie, F. E. Karasz and G. S. Attard, *Macromolecules*, 1992, **25**, 1278.
15 C. T. Imrie, F. E. Karasz and G. S. Attard, *Macromolecules*, 1993, **26**, 545.
16 A. A. Craig, I. Winchester, P. C. Madden, P. Larcey, I. W. Hamley and C. T. Imrie, *Polymer*, 1998, **39**, 1197.
17 K. S. Ryder, D. G. Morris and J. M. Cooper, *Langmuir*, 1996, **12**, 5681.
18 Y. Chen, C. T. Imrie, J. M. Cooper, A. Glidle, D. G. Morris and K. S. Ryder, *Polym. Int.*, 1998, **47**, 43.
19 Y. Nabeshima, A. Shishido, A. Kanazawa, T. Shiono, T. Ikeda and T. Hiyama, *Chem. Mater.*, 1997, **9**, 1480.
20 C. T. Imrie and L. Taylor, *Liq. Cryst.*, 1989, **6**, 1.
21 C. T. Imrie, *Trends Polym. Sci.*, 1995, **3**, 22.
22 C. J. Pickett, K. S. Ryder and J.-C. Moutet, *J. Chem. Soc., Dalton Trans.*, 1993, 3695.
23 F. H. Allen and O. Kennard, *Chem. Design Automat. News*, 1993, **1**, 31.
24 M. R. DuBois, L. D. Vasquez, L. Peslherbe and B. C. Noll, *Organometallics*, 1999, **18**, 2230.
25 Li. Chunbang, S. Serron, S. P. Nolan and J. L. Petersen, *Organometallics*, 1996, **15**, 4020.
26 G. Huttner and O. S. Mills, *Chem. Ber.*, 1972, **105**, 301.
27 H. Yuge, Y. Noda and T. Iwamoto, *Inorg. Chem.*, 1996, **35**, 1842.
28 H. A. M. Biemans, C. Zhang, P. Smith, H. Kooijman, W. J. J. Smeets, A. L. Spek and E. W. Meijer, *J. Org. Chem.*, 1996, **61**, 9012.
29 R. J. Cernik, W. Clegg, C. R. A. Catlow, G. Bushnell-Wye, J. V. Flaherty, G. N. Greaves, I. Burrowes, D. J. Taylor, S. J. Teat and M. Hamichi, *J. Synch. Rad.*, 1997, **4**, 279.
30 SMART and SAINT software for area-detector diffractometers, 1999, Siemens Analytical X-ray Systems, Madison, Wisconsin, USA.
31 G. M. Sheldrick, SADABS (program for scaling and correction of area detector data), 1997, University of Göttingen, Germany.
32 *International Tables for Crystallography*, Kluwer Academic Publishers, Dordrecht, The Netherlands, 1992, **vol. C**, Tables 4.2.6.8 and 6.1.1.4.
33 G. M. Sheldrick, SHELXS-86 User Guide, 1997, University of Göttingen, Germany.
34 G. Ferguson, C. Glidewell, R. M. Gregson and E. S. Lavender, *Acta Crystallogr., Sect. B: Struct. Sci.*, 1999, **55**, 573.
35 G. M. Sheldrick, SHELXL-97 User Guide, 1997, University of Göttingen, Germany.
36 R. Goddard, O. Heinemann and C. Kruger, *Acta Crystallogr., Sect. C: Cryst. Struct. Commun.*, 1997, **53**, 1846.
37 M. Ishihara, M. Tonogaki, S. Ohba, Y. Saito, M. Okazaki, T. Katoh and K. Kamiyama, *Acta Crystallogr., Sect. C: Cryst. Struct. Commun.*, 1992, **48**, 184.
38 R. L. Beddoes, L. Dalton, J. A. Joule, O. S. Mills, J. D. Street and C. I. F. Watt, *J. Chem. Soc., Perkin Trans.*, 1986, 787.
39 H. Korner and P. Zugenmaier, *Cryst. Res. Technol.*, 1997, **32**, 353.
40 K. W. Muir, C. S. Rodger, D. G. Morris and K. S. Ryder, *Acta Crystallogr., Sect. C: Cryst. Struct. Commun.*, 1998, **54**, 1546.
41 D. G. Morris, K. S. Ryder and R. A. Howie, *Acta Crystallogr., Sect. C: Cryst. Struct. Commun.*, 1998, **54**, 1542.